

# Effects of applied electric field and microchannel wetted perimeter on electroosmotic velocity

Subhashish Dasgupta · Ali Asgar S. Bhagat ·  
Marc Horner · Ian Papautsky · Rupak K. Banerjee

Received: 2 May 2007 / Accepted: 27 September 2007 / Published online: 6 November 2007  
© Springer-Verlag 2007

**Abstract** Parameters which affect electroosmotic flow (EOF) behavior need to be determined for characterizing flow in miniature biological and chemical experimental processes. Several parameters like buffer pH, ionic concentration, applied electric field and channel dimensions influence the magnitude of the electroosmotic flow. We conducted numerical and experimental investigations to determine the impact of electric field strength and wetted microchannel perimeter on EOF in straight microchannels of rectangular cross-section. Deviation from theoretical behavior was also investigated. In the numerical model, we solved the continuity and Navier–Stokes equations for the fluid flow and the Gauss law equation for the electric field. Computational results were validated against experimental data for PDMS–glass channels of different wetted perimeters over a range of applied electric fields. Results show that increasing the applied electric field at constant wetted perimeter caused the electroosmotic mobility, the ratio of electroosmotic velocity to applied electric field, to increase nonlinearly. It was also found that increasing the wetted perimeter at constant applied electric field decreased the electroosmotic flow. These findings will be useful in determining the optimum value of the electric field

required to produce a desired electroosmotic flow rate in a channel of a particular dimension. Alternately, these will also be useful in determining the optimum channel dimensions to provide a desired electroosmotic flow rate at a specified value of the electric field.

**Keywords** Electroosmotic velocity · Electroosmotic mobility · Electric field · Wetted perimeter · Zeta potential

## 1 Introduction

Electroosmosis is an electrokinetic flow phenomenon, which can be conveniently used to transport and mix reagents in miniaturized biological and chemical systems. Electroosmotic flow (EOF) occurs when the electric double layer (EDL) near a solid–liquid interface imparts a momentum by an external electric field (Probstein 2003). The momentum then penetrates into the bulk of the liquid by viscous interactions. Most solid surfaces acquire electrostatic charges or an electrical surface potential (Li 2004) in contact with an aqueous solution. The charged solid surface attracts the counter ions (oppositely charged ions) from the liquid towards itself. The counter ions form a dense, mobile layer near the solid surface. The co-ions (like charged ions) mostly remain in the bulk of the fluid. Therefore, there is a net nonzero charge (excess counterions) in the region close to the surface. This net charge balances the charge at the solid surface. The charged surface and the layer of liquid containing the balancing charges are commonly referred to as the EDL.

The EOF offers a number of advantages over pressure-driven microflows (Devasenathipathy and Santiago 2003). Absence of moving parts, such as microscale pumps and

---

S. Dasgupta · R. K. Banerjee (✉)  
Department of Mechanical, Industrial and Nuclear Engineering,  
University of Cincinnati, 688 Rhodes Hall, ML 0072,  
Cincinnati, OH 45221, USA  
e-mail: rupak.banerjee@uc.edu

A. A. S. Bhagat · I. Papautsky  
Department of Electrical and Computer Engineering,  
University of Cincinnati, Cincinnati, OH 45221, USA

M. Horner  
ANSYS Inc, Evanston, IL 60201, USA

valves, simplifies reagent transportation and mixing, and also the systems are easy to fabricate and maintain. In EOF, the velocity of the liquid normal to the cross section is uniform all across it (plug profile). This reduces the chances of sample dispersion (because all particles across a cross-section have the same velocity), as compared to pressure-driven flows, which are characterized by parabolic velocity profiles. Electrophoresis is a phenomenon opposite to electroosmosis, and involves motion of suspended charged species in solution under the influence of an applied electric field. A detailed understanding of the physics of EOF is crucial in designing complex microsystems. Both experimental and numerical investigations are needed to facilitate the development of electrokinetically driven microsystems.

The EOF is influenced by the applied electric field across the two ends of the microchannel, just as the flow rate of a fluid is influenced by a pressure gradient across the ends of a pipe in a pressure-driven system. Terabe et al. (1985), Fujiwara et al. (2002), and Chaiyasut et al. (1999) investigated the relationship between electroosmotic velocity and applied electric field. Numerical studies have been performed to determine the effect of microchannel dimensions on EOF characteristics. Karimi et al. (2003) studied the effect of channel hydraulic diameter and aspect ratio on electroosmotic mobility ( $\mu_{eo}$ ). They found that as the channel hydraulic diameter is increased, it takes a longer period for the flow to become steady. Over the years, numerical calculations of EOF to study electroosmotic flow characteristics have gained prominence. Yang and Li (1998) and Arunandalam and Li (2000) simulated EOF in rectangular microchannels. Qiao et al. (2002) analyzed flow rate and pressure distribution in Microsystems, driven by either electric field or a combination of an electric field and a pressure gradient. Dutta et al. (2002) obtained numerical simulation results for pure electroosmotic and combined electroosmotic/pressure-driven Stokes flow in cross-flow and at Y-split junctions. Yao (2003) developed a computational model to simulate EOF in microsystems. Hu et al. (2003) developed a 3D finite-volume based numerical model to simulate electroosmotic transport in rough microchannels with rectangular prism rough elements on the surfaces. Rawool and Mitra et al. (2006) simulated EOF in serpentine microchannels, subjected to a voltage perpendicular to the flow direction. Krishnamoorthy et al. (2006) numerically simulated EOF in channels of trapezoidal cross-section to understand the impact of surface modifications as well as buffer pH on EOF and sample dispersion.

In the first phase of our investigation, the influence of applied electric field on electroosmotic mobility and hence electroosmotic flow rate was studied. Experiments were carried out in PDMS-glass microchannels measuring

70  $\mu\text{m}$  high and 50 and 100  $\mu\text{m}$  wide. Four different electric field values were investigated: 50, 125, 250 and 500 V/cm. The buffer pH was fixed at 8 for all runs. We investigated the influence of microchannel wetted perimeter in the second phase. The wetted perimeter was changed by varying microchannel widths from 10 to 200  $\mu\text{m}$ , for a constant channel height of 70  $\mu\text{m}$ . We establish the validity and accuracy of this work by comparing and contrasting experimental and computational results in both phases of the above research.

## 2 Methods

### 2.1 Computation methodology

#### 2.1.1 Geometry

Microchannels of rectangular cross-section, filled with a buffer as shown in Fig. 1, were considered. The height of the channels was fixed at 70  $\mu\text{m}$ , the length at 2 cm and the width was varied from 10 to 200  $\mu\text{m}$ . A computational mesh was generated using the pre-processor GAMBIT v. 2.3 (ANSYS Inc., Canonsburg, PA, USA). The mesh was composed entirely of hexahedral (brick) elements. A total of 60,000 elements were used.

#### 2.1.2 Material properties

A buffer with density 1,000  $\text{kg/m}^3$ , dynamic viscosity of 0.001  $\text{N s/m}^2$  and relative permittivity of 80 was used for the calculations.

#### 2.1.3 Governing equations

The governing equations for electroosmotic fluid flow are conservation equations for mass (continuity equation, Eq. 1) and momentum (Navier–Stokes equations, Eq. 2)

$$\nabla \cdot \mathbf{u} = 0 \quad (1)$$

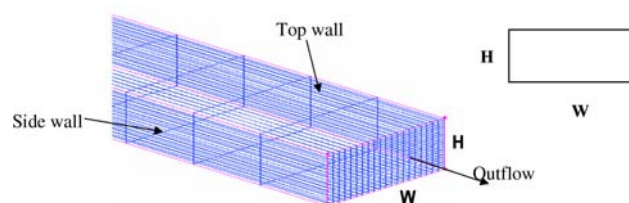


**Fig. 1** The computational grid for solving the electroosmotic flow in straight channels.  $W$  is the channel width and  $H$  is the channel height

$$\rho_m (du/dt + u \cdot \nabla u) = \mu \nabla^2 u - \nabla p + f_e \tag{2}$$

where  $u$  is the velocity vector (cm/s),  $p$  is the pressure (dynes/cm<sup>2</sup>),  $\rho_m$  is the density of the buffer solution (g/cm<sup>3</sup>), and  $\mu$  is the dynamic viscosity (dynes/cm<sup>2</sup>) of the buffer. The last term,  $f_e$ , is the Coulomb force term, arising due to application of an external electric field on wall charges.

$$f_e = \rho_e E \tag{3}$$

where  $\rho_e$  is the bulk charge density (C/cm<sup>2</sup>),  $E$  is the electric field (V/cm). The wall charge is modeled as a slip boundary condition applied at the walls. Since  $\rho_e = 0$ , the Coulomb force term is zero in our formulation.

The governing equation for the electric field is the Gauss law equation:

$$\nabla \cdot (\sigma \nabla \phi) = -\rho_e \tag{4}$$

where  $\phi$  is the applied voltage (V) and  $\sigma$  is the electric conductivity of the buffer (Siemens/cm). Since bulk charge in the buffer is zero, we have that  $\rho_e = 0$ . Substituting in Eq. 4

$$\nabla^2 \phi = 0 \tag{5}$$

From Eq. 5, the Electric field is calculated in 3D space by a subroutine as

$$E = \nabla \phi \tag{6}$$

### 2.1.4 Boundary conditions

Boundary conditions for the voltage and the fluid velocity at the walls are required to close the system of equations. The voltage is specified at the inlet and outlet of the microchannel. For the flow equations, the computational model is greatly simplified if one does not have to resolve the velocity field in the EDL. This situation may be avoided when the thickness of the EDL, known as the Debye layer, is small relative to the channel height and width. The Debye layer thickness  $\lambda_D$  is (Li 2004)

$$\lambda_D = (3.04/zM^{1/2}) \times 10^{-10} \tag{7}$$

where  $z$  is the valence of the ion(s) and  $M$  is molarity (mol/L). For 20 mM phosphate buffer and  $z = +1$  (or whatever

number is relevant for this investigation),  $\lambda_D$  is 2.15 nm and  $\lambda_D/W = 2.15 \times 10^{-4}$  which is negligible. Thus, a slip boundary condition can be applied on the walls of the microchannel with minimal impact on the accuracy of the flow solution. We refer to Dutta et al. (2002) according to which a slip flow at the boundary can be imposed to approximate the effect of the charged layer. The Kn or Khudsen number in our case varies from  $10^{-3}$  to  $10^{-5}$ . The slip flow regime is,  $10^{-3} < Kn < 0.1$  that is applicable to gas flows in micro systems. However, we refer to Dutta et al. (2002) according to which a slip flow at the boundary can be imposed to approximate the effect of the charged layer. The slip-velocity was calculated from the Helmholtz–Smoluchowski equation (Probstein 2003):

$$U_{eo} = -\zeta \epsilon E / \mu = -\mu_{eo} E \tag{8}$$

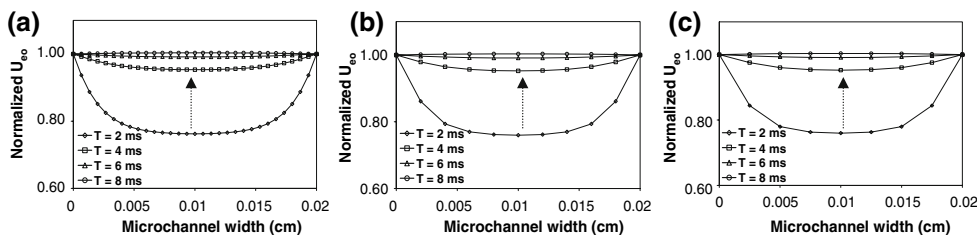
where  $U_{eo}$  is the electroosmotic velocity (cm/s),  $\zeta$  is zeta potential (V),  $\mu_{eo}$  is the numerical electroosmotic mobility and  $E$  is the electric field calculated in a subroutine by Eq. 6. It can be observed that  $\zeta$  is an input parameter that was calculated from the experimental electroosmotic mobility  $\mu'_{eo}$ . Details are given in Sect. 9.

### 2.1.5 Finite element method

The governing equations were discretized and solved using a finite element method (FIDAP). This method provides a unique advantage of the use of subroutines to resolve the electric field in 3D space. The numerical electric field can be used to calculate the slip velocity at the walls imposed as a boundary condition. A low-memory segregated solver was used to perform the calculations. Iterations proceeded until the relative change in the solution was less than  $1/e^6$  from one iteration to the next. Mesh independence was ensured by comparing the velocity profiles in the microchannel at different cross-stream aspect ratios of 5, 11 and 20 (Fig. 2). There was a difference of less than 0.1% in the minimum velocities attained by the buffer. Thus, the aspect ratio of the mesh elements was kept constant at 11 in the cross-stream direction.

Figure 3 shows a three image sequence indicating the velocity profile of the buffer within the microchannel.

**Fig. 2** Similar velocity profiles at aspect ratios **a** 5, **b** 11, **c** 20 indicate mesh independence for the 200 μm wide channel



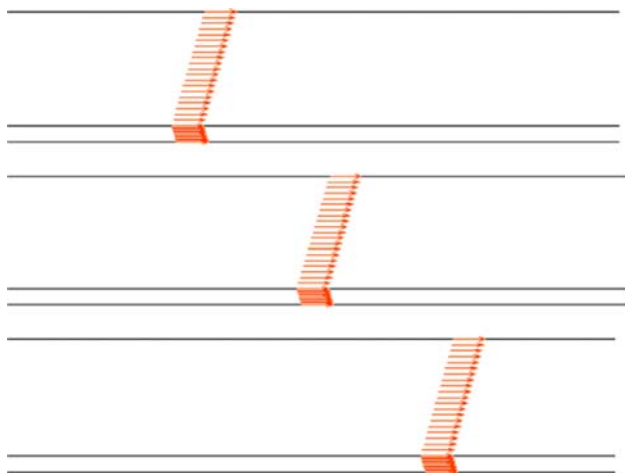


**Fig. 3** Typical velocity profiles of electroosmotic flows in microchannels using the finite element method

## 2.2 Experimental methodology

### 2.2.1 Fabrication

Initially, 3 in. silicon wafers was cleaned with acetone, methanol and DI water for 3 min each followed by a 12 min piranha clean [7:3 mixture (*v/v*) of  $\text{H}_2\text{SO}_4\text{:H}_2\text{O}_2$ ]. Following the piranha clean, wafers were rinsed with DI water for a few minutes and dipped in Buffered Oxide Etchant (BOE, 3:3:1 (*v/v/v*),  $\text{H}_2\text{O:NH}_4\text{F:HF}$ ) for 15 s to remove any native oxide layer from the surface, and then rinsed with DI water. Next, wafers were blown dry using  $\text{N}_2$ , dehydrated on a leveled hotplate at  $150^\circ\text{C}$  for 20 min, and then cooled to room temperature before spin-coating them with the photoresist.

Wafers were then coated with a negative photoresist, SU-8 2075 (MicroChem Corp., MA, USA), to define the  $70\ \mu\text{m}$  microchannels and SU-8 2035 to define the  $35\ \mu\text{m}$  microchannels. Following spin coating, the wafers were transferred onto a level surface for 10 min to allow the photoresist to relax. The pre-bake was then performed on a temperature-controlled level hot plate (SU-8 2075:  $65^\circ\text{C}$  for 10 min and  $95^\circ\text{C}$  for 45 min, SU-8 2035:  $65^\circ\text{C}$  for 5 min and  $95^\circ\text{C}$  for 10 min). The wafers were then gradually cooled to room temperature by turning off the heater

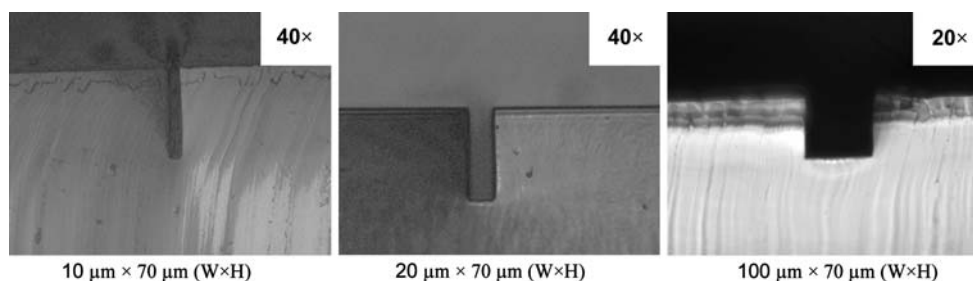
and leaving the wafers on the hot plate for 15–20 min. The resist was exposed for 35 s at  $5\ \text{mW}/\text{cm}^2$  using an I-line (365 nm) high pass filter. Glycerin was used during exposure to reduce any diffraction effects ( $\sim 750\ \mu\text{L}$  for 3 in. wafer) that may arise due to surface roughness. Postexposure bake was then carried out on a level hot plate (SU-8 2075:  $65^\circ\text{C}$  for 5 min and  $95^\circ\text{C}$  for 15 min, SU-8 2035:  $65^\circ\text{C}$  for 1 min and  $95^\circ\text{C}$  for 3 min). The wafers were then developed in the SU-8 developer (MicroChem Corp.). To confirm development, the wafers were rinsed with isopropyl alcohol. Following development, wafers were rinsed with DI water, blown dry using  $\text{N}_2$  and de-scummed in  $\text{O}_2$  plasma (20 sc cm, 13.56 MHz) for 2 min at 300 W to clean the wafer off any residual photoresist.

The patterned wafers were treated with Sigmacote (Cat # SL-2, Sigma Aldrich) to facilitate PDMS mold release. The PDMS was mixed at a 10:1 (m/m) ratio of elastomer base to curing agent. The mixture was degassed and poured over the photoresist molds to achieve a 1 mm thickness. The PDMS was cured at  $80^\circ\text{C}$  for 2.5 h on a level hotplate. After curing, the PDMS molds were cut and peeled from the masters with a sharp razor blade or scalpel. The inlet and outlet reservoirs were carefully pierced using a 2 mm (OD) punch, and excess PDMS was removed from the molds. Microscope glass slides (1 in.  $\times$  3 in.) and the PDMS molds were cleaned in 1:5 (*v/v*) ratio of  $\text{HCl:H}_2\text{O}$  for 12 min and blown dry using  $\text{N}_2$ . The PDMS molds were then bonded to the glass slides by exposing both of them to  $\text{O}_2$  plasma (20 sc cm, 13.56 MHz) for 15 s at 70 W (Jo et al. 2000). Following plasma treatment, the surfaces were immediately brought into contact with each other and placed on a hotplate at  $85^\circ\text{C}$  for 2 h to complete the bonding. Figure 4 shows microscopic images of the cross-sections of microchannels fabricated in PDMS.

### 2.2.2 Characterization

The current monitoring method was used to measure the  $\mu_{\text{eo}}$  in fabricated channels. This method (Li 2004) measures the time required for a dilute buffer to displace a more concentrated buffer (and vice versa) in the entire microchannel. As the dilute buffer replaces the concentrated

**Fig. 4** Microscopic images showing the cross-sections of the different microchannels fabricated in PDMS for this study



buffer, the current across the channel keeps decreasing, because the concentrated buffer has higher conductivity. After the entire concentrated buffer is replaced by the dilute buffer, the current essentially remains constant. Figure 5 shows the experimental set-up for these measurements. It consists of the microchannels, two platinum electrodes (at inlet and outlet reservoir), a high voltage power supply (HVS448, Labsmith) and data acquisition system to measure the current driven using a custom LabVIEW program. All measurements were conducted using 10 and 20 mM phosphate buffers (pH 8). Prior to testing, all channels were treated with 1 M NaOH solution for 5 min. Figure 6 shows example of current-time plots obtained using the LabVIEW program. From the plot, the time required ( $T_{EOF}$ ) for the 10 mM buffer to replace the 20 mM buffer (and vice versa) is recorded. The experimental  $\mu'_{eo}$  is then given by

$$\mu'_{eo} = \frac{L}{E' \times T_{EOF}} \quad \text{cm}^2/\text{V s} \quad (9)$$

$$E' = (\phi_{inlet} - \phi_{outlet})/L \quad \text{V/cm} \quad (10)$$

where  $L$  (cm) is the length of the microchannel (cm),  $T_{EOF}$  (s) is the time required for one buffer to displace the other,  $E'$  (V/cm) is the approximate applied electric field,  $L$  is length of channel and  $\Phi_{inlet}$  and  $\Phi_{outlet}$  are the electric potentials at the inlet and outlet, respectively. The zeta potential,  $\zeta$ , is calculated from  $\mu'_{eo}$  by applying the Helmholtz–Smoluchowski equation (Probstein 2003).

### 3 Results and discussion

Results of experiments and theoretical predictions for the different microchannel cross-sections and applied electric fields are shown in Table 1. The reproducibility of experiments was confirmed by comparing experimental results measured on three different days under the same conditions. It is seen that for most of the cases there is a significant difference between experimental and theoretical velocities, the maximum being 86.5% in the 100  $\mu\text{m}$  wide channel at  $E = 62.5$  V/cm. This is discussed in the following sections.

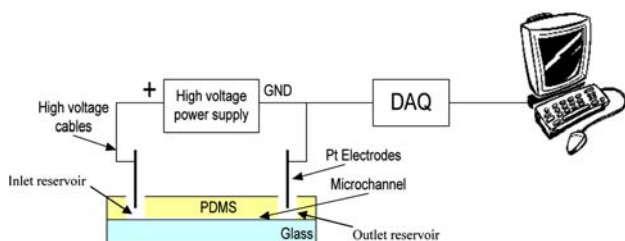


**Fig. 5** Experimental set-up to measure the electroosmotic mobility of microchannels using the current monitoring method

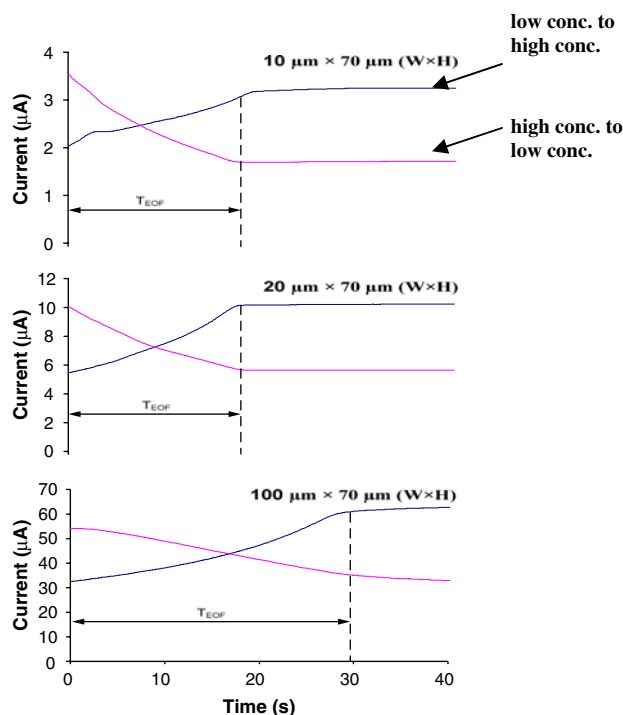


**Fig. 6** Current-time plots for current monitoring measurement of electroosmotic flow. Phosphate buffers (pH 8) of 10 and 20 mM concentration are used at an applied electric field of 250 V/cm. The buffer replacement time ( $T_{EOF}$ ) is then measured from the plot to calculate the electroosmotic mobility

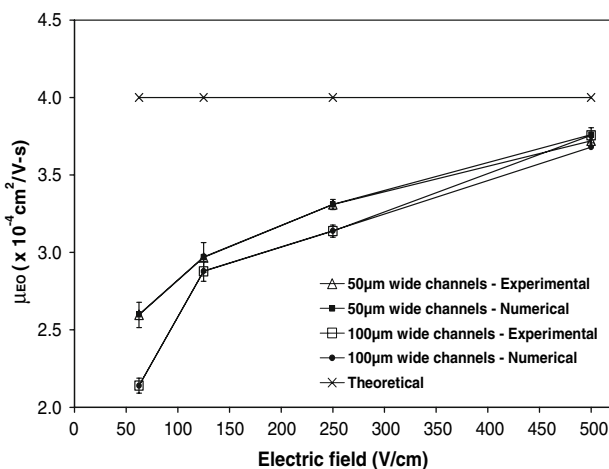
#### 3.1 Effect of applied electric field

Figure 7 shows the effect of applied electric field on electroosmotic mobility, for channels of width 50 and 100  $\mu\text{m}$ . The experimental and numerical results were in good agreement (<2% error) (Fig. 7). It has been found experimentally that there is a rise in electroosmotic mobility ( $\mu_{eo}$ ) with applied electric field throughout the range considered (50 to 500 V/cm) contrary to theoretical predictions (Fig. 7). Terabe et al. (1985) found experimentally that electroosmotic velocity had a nonlinear relationship with applied voltage. They measured the temperature rise across the fused silica tube used in their experiments and found that it was 45°C higher than the ambient temperature at an applied electric field of  $\sim 410$  V/cm. They concluded that Joule heating decreases the viscosity of the liquid. Ross et al. (2001) drew similar conclusions from their experimental results. Fujiwara et al. (2002) experimentally investigated into the effect of applied electric field on EOF in a donut-shaped channel and found that electroosmotic velocity is not linearly proportional to applied electric field (contrary to the Helmholtz–Smoluchowski equation) and thus  $\mu_{eo}$  changes with the applied electric field. They found that electroosmotic mobility is constant up to 50 V/cm, decreases from



**Table 1** Theoretical and experimental electroosmotic velocity for various tested conditions (channel height = 70  $\mu\text{m}$ )

S. no.	Channel width ( $\mu\text{m}$ )	Electric field (V/cm)	Experimental velocity (cm/s)	Theoretical velocity (cm/s)	% Deviation from expt. velocity
1	10	250	0.113	0.1	11.5
2	10	500	0.2615	0.2	23.5
3	20	250	0.104	0.1	3.84
4	20	500	0.226	0.2	11.5
5	50	62.5	0.01625	0.025	53.8
6	50	125	0.0371	0.05	34.7
7	50	250	0.085	0.1	17.6
8	50	500	0.188	0.2	6.38
9	100	62.5	0.0134	0.025	86.5
10	100	125	0.036	0.05	38.8
11	100	250	0.078	0.1	28.2
12	100	500	0.185	0.2	8.1
13	200	250	0.071	0.1	40.8
14	200	500	0.18	0.2	11

**Fig. 7** Numerical and experimental results indicating the effect of electric field ( $E$ ) on electroosmotic velocity ( $U_{eo}$ ) for 50 and 100  $\mu\text{m}$  wide channels (height = 70  $\mu\text{m}$ ). The *hashed line* indicates the  $\mu_{eo}$  calculated using Helmholtz Smoluchowski equation

50 to 140 V/cm and then remains constant upto 260 V/cm. One possible explanation is the Joule heating effect which decreases the viscosity of the liquid. However, upon measurement they found that there was only 0.5°C rise of temperature across the donut channel. According to them, the  $\zeta$  varies with electric field. They concluded that the variation in  $\zeta$  is due to the variation in concentration of charges in the electric double layer with applied electric field. Krishnamoorthy et al. (2006) theoretically calculated the temperature rise across surface modified channels to be 0.4°C, and concluded that Joule heating was negligible. For our channels of maximum cross-sectional dimension

$d = 200 \mu\text{m}$ , the maximum temperature rise due to Joule heating can be expressed as (Ramos et al. 1998)

$$\Delta T = \sigma E^2 d^2 / 8k \quad (11)$$

where  $T$  is the temperature in Kelvin,  $k$  is thermal conductivity of 0.6062 W/mk (equivalent to that of water),  $\sigma$  is electrical conductivity, and  $E$  is maximum field strength. For our case of 10 mM phosphate buffer ( $\sigma = 0.17 \text{ S/m}$ ) and electric field strength ( $E = 500 \text{ V/cm}$ ), the maximum temperature rise is calculated to be 3.5°C, which is an insignificant rise. Thus, the only possibility is that at higher electric fields a secondary charged layer develops behind the primary charged layer (Kremer and Richtering 2004), thereby increasing the overall zeta potential of the surface. These findings are in contrast with theoretical predictions based on Helmholtz–Smoluchowski equation (Eq. 7), according to which electroosmotic velocity,  $U_{eo}$ , increases linearly with  $E$ . In other words, for this scenario, electroosmotic mobility  $\mu_{eo}$ , is independent of applied  $E$ . For 50  $\mu\text{m}$  wide channels,  $\mu_{eo}$  varied from theoretical predictions by 6.4 to 53.8% (Table 1) for increasing electric fields. Similarly for 100  $\mu\text{m}$  wide channels, 8.1 to 86.5% (Table 1) variations from theoretical values were observed. For theoretical predictions, the electroosmotic mobility of  $4\text{E-}4 \text{ cm}^2/\text{V s}$  was taken from Spehar et al. (2003) at ionic strength of 20 mM for PDMS/glass microchannel.

Thus, we confirm from experimental evidence and numerical calculations that electroosmotic velocity increases nonlinearly with increasing applied electric field, due to modification of the surface charge and hence, the zeta potential. It should also be noted that the  $U_{eo}$  for channels of 100  $\mu\text{m}$  widths is less than channels of 50  $\mu\text{m}$  width under the same buffer conditions and for the same applied electric field. We will discuss this effect subsequently.

### 3.2 Effect of wetted perimeter

The effect of channel wetted perimeter has been numerically and experimentally investigated. Not many investigations, relating channel dimensions and EOF characteristics, have been done previously. Karimi and Culham (2003) found by numerical calculations that as the hydraulic diameter of the channel increases,  $\mu_{eo}$  decreases. They concluded that as the hydraulic diameter increases it takes a longer time for the flow to become steady. In our investigations the width of the channel was varied to change the channel wetted perimeter ( $2W + 2H$ ), where  $W$  is the width and  $H$  is the height of the microchannel. Figure 8 shows the effect of channel width on,  $\mu_{eo}$ , and compares numerical and experimental results. It is found that as the wetted perimeter increases the  $\mu_{eo}$  decreases. It should be noted that the gradient of the curve decreases

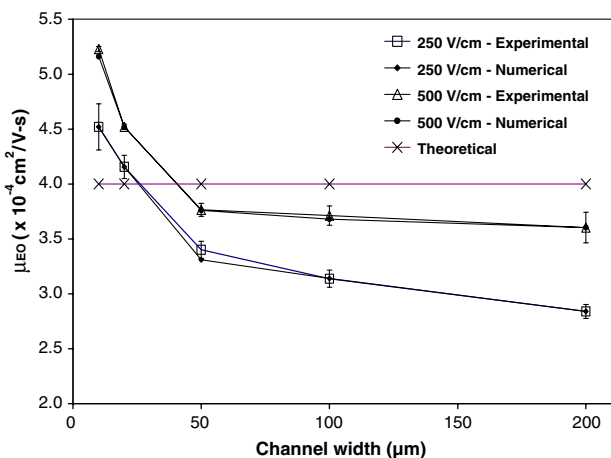


**Fig. 8** Numerical and experimental results indicating the effect of channel width on electroosmotic mobility for 250 and 500 V/cm electric fields, respectively. The height of the channels is fixed at 70 μm. Good agreement (<2%) between numerical and experimental results was obtained

with increasing channel width. The numerical calculations and experimental results match well (<2%). However, theoretical predictions show no effect of channel dimensions on  $\mu_{eo}$  or  $U_{eo}$ . For 250 V/cm input, experimental  $\mu_{eo}$  varies from 3.84 to 40.8% (Table 1) from theoretical predictions as the microchannel width increases from 10 to 200 μm. Similarly, for a 500 V/cm input, the error between experimental and theoretical predictions varied from 6.38 to 23.5% (Table 1). The discrepancy is due to two effects: (1) for wider channels, the momentum transfer from the

surface of the channel to the core takes a longer time; and (2) an increase in channel width and a consequent increase in liquid volume result in inertia forces gaining predominance over electroosmotic forces. It should be noted that in calculating the theoretical mobility, we assumed that the inertia terms can be neglected in the governing equations. Thus, there is substantial variation between theoretical mobility and experimental and numerical mobilities.

Figure 9 shows electroosmotic velocity profiles generated by computations in channels of widths 10, 50 and 100 μm at different instances of time. The velocity plots have been normalized with respect to the slip velocity at the walls. In the 10 and 50 μm wide channels the profiles change from that of a near inverse parabola to a steady state plug profile in 0.0015 and 0.003 s, respectively. However, in case of the 200 μm wide channel, it takes 0.008 s to attain a steady state. This is because in wider channels the electroosmotic force takes a longer time to penetrate the core of the channel. We see that larger the channel width the longer it takes to attain a steady state profile. It is expected that at a higher channel width the electroosmotic force will not be able to overcome the inertia force required to move the fluid within the microchannel. This has also been observed in our experiments.

We have also investigated the effect of aspect ratio of microchannel on  $\mu_{eo}$ . Table 2 shows  $\mu_{eo}$  at different channel dimensions (wetted perimeter), at constant aspect ratios of 0.7 and 0.35. We found that there is no significant relation between aspect ratio and electroosmotic mobility, because at the same aspect ratio there is considerable

**Fig. 9** Electroosmotic velocity profiles in channels of widths **a** 10 μm, **b** 50 μm and **c** 200 μm. Dotted arrows indicate direction of flow of buffer

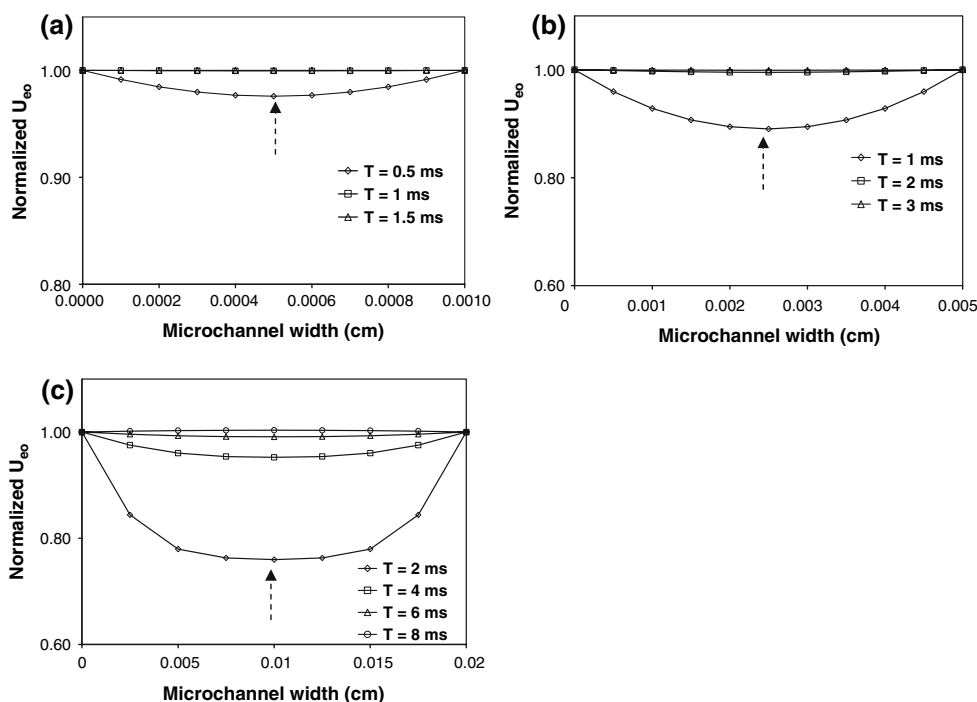


**Table 2** Effect of aspect ratio on electroosmotic mobility ( $E = 250 \text{ V/cm}$ )

Channel width ( $\mu\text{m}$ )	Channel height ( $\mu\text{m}$ )	Aspect ratio	EOF mobility ( $\text{cm}^2/\text{V s}$ )
100	70	0.7	3.14E-04
50	35	0.7	3.89E-04
200	70	0.35	2.84E-04
100	35	0.35	3.56E-04

difference in  $\mu_{eo}$ , for different wetted perimeters. Therefore, it is wetted perimeter of the microchannel, which has a significant influence on  $\mu_{eo}$ .

#### 4 Conclusion

The EOF in channels of varying wetted perimeters and under the influence of varying applied electric field has been studied both numerically and experimentally. The numerical and experimental results have matched within 2% of each other. The influence of applied electric field and channel wetted perimeter on  $U_{eo}$  was investigated experimentally and numerically, and deviations from theoretical behavior were compared. Contrary to theoretical predictions,  $U_{eo}$  rises nonlinearly with applied electric field. As Joule heating was found to be insignificant, the nonlinear rise of  $U_{eo}$  with electric field is attributed to increase in zeta potential due to formation of a secondary charged layer behind the primary one. Further, microchannel wetted perimeter has a significant effect on  $U_{eo}$ , which decreases with increasing wetted perimeter. This is, again, contrary to theoretical predictions according to which there is no effect of microchannel dimensions on  $U_{eo}$ . For wider channels, electroosmotic forces take longer time to penetrate from the surface of the channel to the bulk of the fluid buffer. With increase in channel width the inertial forces dominate in comparison to the electroosmotic forces. Lastly, it was found that aspect ratio did not have a significant relationship with  $\mu_{eo}$ . With the recent trend of reducing channel dimensions towards nanofluidics, we believe these results will be valuable in designing EOF-based microfluidic systems. Future work can be done to investigate the effect of channel shape on electroosmotic flow characteristics both experimentally and computationally.

**Acknowledgments** The authors gratefully acknowledge support from the University of Cincinnati Institute for Nanoscale Science and Technology.

#### References

- Arunandalam S, Li D (2000) Liquid transport in rectangular microchannels by electroosmotic pumping. *Colloids Surf A Physicochem Eng Asp* 161(1):89–102
- Chaiyasut C, Tsuda T, Kitagawa S, Wada H, Nakabeya Y (1999) Pressure flow driven electrochromatography using fluorinated bonded silica. *J Microcolumn Sep* 11(88):590–595
- Devasenathipathy G, Santiago JG (2003) Micro- and nano-scale diagnostic techniques. In: Breuer KS (ed). Springer, New York
- Dutta P, Bestok A, Warburton TC (2002) Electroosmotic flow control in complex microgeometries. *J Microelectromech Syst* 2(1):36–44
- Fujiwara T, Kitoh O, Tsuda T (2002) Effect of parallel applied electric field on electroosmotic flow in donut channel. *Chromatography* 23(1):25–31
- Hu Y, Werner C, Li D (2003) Electrokinetic transport through rough microchannels. *Anal Chem* 75(21):5747–5758
- Jo BH, Van Lerbergh LM, Motsegood KM, Beebe DJ (2000) Three-dimensional micro channel fabrication in polydimethylsiloxane (PDMS) elastomer. *J Microelectromech Syst* 9:76–81
- Karimi G, Culham JR (2003) Transient electro-osmotic pumping in rectangular microchannels. MEMS, NANO and Smart Systems, 2003. Proceedings international conference, pp 364–372
- Kremer F, Richtering W (2004) Progress in colloid and polymer science, vol 128. Springer, Heidelberg
- Krishnamoorthy S, Feng J, Henry AC, Locasio LE, Hickman JJ, Sundaram S (2006) Simulation and experimental characterization of electroosmotic flow in surface modified channels. *Microfluid Nanofluid* 2:345–355
- Li D (2004) Electrokinetics in microfluidics. Elsevier, Amsterdam
- Probstein RF (2003) Physicochemical hydrodynamics: an introduction. Wiley, New York
- Qiao R, Aluru NR (2002) A compact model for electroosmotic flows in microfluidic devices. *J Micromech Microeng* 12(5):625–635
- Ramos A, Morgan H, Green NG, Castellanos A (1998) Ac electrokinetics: a review of forces in microelectrode structures. *J Phys D Appl Phys* 31(18):2338–2353
- Rawool AS, Mitra SK (2006) Numerical simulation of electroosmotic effect in serpentine channels. *Microfluid Nanofluid* 2(3):261–269
- Ross D, Johnston T, Locasio LE (2001) Imaging of electroosmotic flow in plastic microchannels. *Anal Chem* 73(11):2509–2519
- Spehar A-M, Koster S, Lidner V, Kulmala S, de Rooij NF, Verpoorte E, Sigrist H, Thormann W (2003) Electrokinetic characterization of poly(dimethylsiloxane) microchannels. *Electrophoresis* 24:3674–3678
- Terabe S, Otsuka K, Ando T (1985) Electrokinetic chromatography with miscellar solution and open tubular capillary. *Anal Chem* 57:834–841
- Yang C, Li D (1998) Analysis of electrokinetic effects on the liquid flow in rectangular microchannels. *Colloids Surf A Physicochem Eng Asp* 143(2–3):339–353
- Yao GF (2003) A computational model for simulation of electroosmotic flows in Microsystems. Technical proceedings of the 2003 nanotechnology conference and trade show, vol 1(9), pp 218–221